

Spinor Condensates on a Cylindrical Surface in Synthetic Gauge Fields

Tin-Lun Ho^{1,2} and Biao Huang¹

¹*Department of Physics, The Ohio State University, Columbus, Ohio 43210, USA*

²*Institute for Advanced Study, Tsinghua University, Beijing 100084, China*

(Received 7 May 2015; revised manuscript received 15 September 2015; published 9 October 2015)

We show that by modifying the setup of the recent experiment that creates a “Dirac string” one can engineer a quasi-2D spinor Bose-Einstein condensate on a cylindrical surface, with a synthetic magnetic field normal to the surface. Because of the muticonnectivity of the surface, there are two types of vortices (called *A* and *B*) with the same vorticity. This is very different from the planar case, which only has one kind of vortex for fixed circulation. As the strength of the synthetic gauge field increases, the ground states will form a necklace of alternating *AB* vortices surrounding the lateral midpoint of the cylinder, and will split into two *A* and *B* necklaces at higher synthetic gauge fields. The fact that even the basic vortex structure of a Bose-Einstein condensate is altered in a cylindrical surface implies that richer phenomena are in store for quantum gases in other curved surfaces.

DOI: 10.1103/PhysRevLett.115.155304

PACS numbers: 67.85.-d, 03.75.Lm, 03.75.Mn

In the study of quantum matter, one usually deals with Euclidean space. Spaces with nonzero curvatures are seldom encountered. However, recent studies show that many important properties of many-body systems can be revealed by changing the geometry or topology of the background manifold. For instance, the ground state degeneracy of a quantum Hall system is shifted by an amount proportional to the genus of the manifold [1]. A change of the spatial geometry of the system can also lead to a dissipation-free “Hall viscosity” response in two-dimensional systems [2]. Furthermore, it was found in graphene that curvature effects can mimic those of gauge fields [3]. The fact that manifolds with non-Euclidean geometry can help uncover new features of quantum matter makes it desirable to create manifolds of controllable shape and to develop the capability to add in synthetic gauge fields.

The purpose of this Letter is to discuss how to create quantum gases on curved surfaces with synthetic gauge fields, as well as their properties. As a first step, we consider a spinor Bose-Einstein condensate (BEC) in the form of a cylindrical surface (produced by an annulus trap). Bose condensation will magnify quantum phenomena on the macroscopic scale, while large spins will lead to stronger synthetic gauge fields through Berry phase effects. Our study is an extension of the ongoing effort of generating synthetic gauge fields in quantum gases (using rotating traps [4–10], Raman transitions, or shaking lattices [11–17]) to explore the effect of geometry and topology of the underlying manifold on BECs in such settings [18].

A cylindrical surface has a nontrivial topology (i.e., a hole) and an extrinsic curvature [19]. As we shall see, the nontrivial topology of this surface leads to two types of vortices (denoted as *A* and *B*) with the *same* circulation, in contrast to the single type of vortex for given circulation in

planar geometry. This is because there are only two conformal maps that take a plane into a cylinder that satisfy the topological constraint. We further show that in the presence of a synthetic magnetic field, the confining potential of the annulus will give rise to a “necklace” of vortices—a row of alternating *A* and *B* vortices surrounding the center of the cylinder at $z = 0$, rather than the usual hexagonal vortex array in a planar geometry. Such vortex patterns will show up in time-of-flight experiments as a density distribution with $2n$ -fold rotational symmetry around the axis of the cylinder (n being the number of *A-B* vortex pairs in the ground state), which can be detected easily. The fact that structures as fundamental as vortices can come in different varieties on a cylindrical surface suggests that many new phenomena are in store for more complex curved spaces.

Realization of a BEC on a cylindrical surface in Landau gauge.—To create a quasi-2D BEC in the form of a cylindrical surface, we first create an annulus trap of narrow width by piercing through a trap (produced by a red-detuned laser) with a repulsive potential (produced by a blue-detuned laser), as shown in Fig. 1. This will create a confining well in the radial direction with a minimum at radius R . A harmonic potential $V(z) = M\omega_z^2 z^2/2$ is applied along z . If ω_z is much weaker than the trap frequency in the radial direction, then a quantum gas in this trap will form a quasi-2D cylindrical surface with radius R , thickness σ , and finite height (see Fig. 1 and Ref. [20]).

Next, we insert a quadrupolar magnetic field \mathbf{B} into the center of the cylinder (see Fig. 1), $\mathbf{B}(\mathbf{x}) = B_0(x\hat{x} + y\hat{y} - 2z\hat{z}) = B_0r(\sin\theta\cos\varphi\hat{x} + \sin\theta\sin\varphi\hat{y} - 2\cos\theta\hat{z})$. Such a field configuration was used recently in the experiment by Hall and co-workers [21]. Our configuration is a modification of their setup by piercing through the harmonic potential with a blue-detuned laser. For sufficiently large

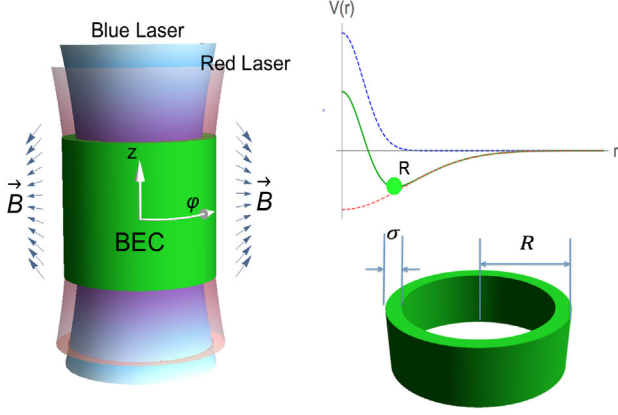


FIG. 1 (color online). The blue and red dotted lines represent the attractive and the repulsive potential due to the red-detuned and blue-detuned lasers. The green curve is the combined potential, with a minimum at R . For sufficiently large R and for weak harmonic confinement along z , the quantum gas will form a quasi-2D cylindrical layer with thickness $\sigma \ll R$, shown in green [20].

B_0 , the low energy space is made up of bosons with spin pointing in the direction of the local field $\mathbf{B}(\mathbf{x})$. Denoting the direction of the spin as $\hat{l} = \cos\beta\hat{z} + \sin\beta(\cos\alpha\hat{x} + \sin\alpha\hat{y})$, we have

$$\alpha = \varphi, \quad \cos\beta = -\frac{2z}{\sqrt{R^2 + 4z^2}}. \quad (1)$$

The condensate wave function of bosons with spin S is then $\psi_a(\mathbf{x}) = \zeta_a(\mathbf{x})\phi(\mathbf{x})$, where a is the spin index and $\zeta_a(\mathbf{x})$ is a normalized vector aligned with the local magnetic field, i.e., $\hat{\mathbf{B}}(\mathbf{x}) \cdot \mathbf{S}_{ab}\zeta_b(\mathbf{x}) = S\zeta_a(\mathbf{x})$.

The energy functional reads (with spin indices suppressed)

$$E[\psi] = \int d^2x \left[\frac{\hbar^2}{2M} |\nabla\psi|^2 - [\mu - V(z)]|\psi|^2 + \frac{g}{2} |\psi|^4 \right]. \quad (2)$$

Here, we have $\nabla = \hat{z}\partial_z + R^{-1}\hat{\varphi}\partial_\varphi$. With $\zeta_a(\mathbf{x})$ frozen by $\mathbf{B}(\mathbf{x})$, Eq. (2) reduces to a functional of $\phi(\mathbf{x})$. The kinetic part becomes

$$|\nabla\psi|^2 = \left| \left(\frac{\nabla}{i} + \frac{\zeta^\dagger \nabla \zeta}{i} \right) \phi \right|^2 + [|\nabla\zeta|^2 + (\zeta^\dagger \nabla \zeta)^2] |\phi|^2. \quad (3)$$

Both $|\nabla\zeta|^2$ and $(\zeta^\dagger \nabla \zeta)^2$ serve as additional harmonic potential around $z = 0$ [22]. We shall then denote the total harmonic trap along z as $V_z = \frac{1}{2}M\bar{\omega}_z^2 z^2$. Thus, the system represents scalar charged bosons $\phi(\mathbf{x})$ moving in synthetic magnetic field, with the gauge potential and field strength $\mathbf{A}_{\text{syn}} = i\zeta^\dagger \nabla \zeta = S(\nabla\alpha) \cos\beta \approx -(\hat{\varphi}/R)(2zS/R)$, $\mathbf{B}_{\text{syn}} = \nabla \times \mathbf{A}_{\text{syn}} \approx (2S/R^2)\hat{\mathbf{r}}$ near $z = 0$. The strength of the

synthetic field is proportional to $2S$, so a vortex ground state is expected for condensates with sufficiently large spin. To simplify notations, we measure length in units of R , so that $z/R \rightarrow z$, and z is now dimensionless. We further introduce the dimensionless variables $\tilde{\alpha} \equiv M\bar{\omega}_z R^2/\hbar$, $\tilde{\mu} \equiv \mu/(\hbar^2/2MR^2)$, $\tilde{g} \equiv g/(\hbar^2/2MR^2)$; then the energy functional becomes $E[\psi] = (\hbar^2/2MR^2) \int d^2x \mathcal{E}$:

$$\mathcal{E} = |\partial_z \phi|^2 + |(-i\partial_\varphi + 2Sz)\phi|^2 - (\tilde{\mu} - \tilde{\alpha}^2 z^2)|\phi|^2 + (\tilde{g}/2)|\phi|^4. \quad (4)$$

The physics in the lowest Landau level (LLL) [23] can provide useful physical intuitions. The noninteracting part of the Hamiltonian in Eq. (4) is

$$h = -\partial_z^2 + (-i\partial_\varphi + 2Sz)^2 + \tilde{\alpha}^2 z^2. \quad (5)$$

It describes a charged particle in a magnetic field in the Landau gauge in the presence of a harmonic potential. The eigenstates in the LLL are $f_m(\varphi, z) = e^{-im\varphi} e^{-\nu(z-z_m)^2/2}$, $z_m = (2S/\nu)m$, $\nu \equiv \sqrt{4S^2 + \tilde{\alpha}^2}$, with energy $\varepsilon_m = \nu + (\tilde{\alpha}^2/\nu^2)m^2$. The state f_m is a ring at z_m with m units of circulation around the azimuthal direction. It is useful to rewrite f_m as

$$f_m(\varphi, z) = C_m w^m e^{-\nu z^2/2}, \quad w = e^{-iu}, \quad (6)$$

$$u = \varphi + i\frac{2S}{\nu}z,$$

where $C_m = e^{-2S^2 m^2/\nu^3}$. Here, u is the complex number that represents the point (φ, z) and w is the conformal map that takes the cylinder (φ, z) into a 2D plane (w_x, w_y) . Equation (6) shows that f_m is a simple power of w apart from the Gaussian in z .

For noninteracting systems, bosons will condense in the $m = 0$ state. However, as in the planar case, an increasing repulsive interaction will change the condensate at $m = 0$ to other linear combinations of m states so as to reduce the repulsion energy. We shall not discuss the vortex transition in the LLL in this Letter. Instead, we point out that a linear combination of the form $B_M \phi_M + B_{-M} \phi_{-M}$ amounts to a linear array of 2π vortices, since $B_M w^M + B_{-M} w^{-M} = B_{-M} w^{-M} \prod_{\ell=1}^{2M} \{w - [-(B_{-M}/B_M)]^{1/2M} e^{i\pi\ell/M}\}$. It is easy to see that a vortex in the w space is also a vortex in the u space.

Isolated vortex on a cylindrical surface.—To bring the discussion closer to current experiments, we consider a gas with $\sim 10^5$ bosons, which typically occupy many Landau levels. If $\phi(\varphi, z)$ has a vortex at $u_j = \varphi_j + i(2S/\nu)z_j$ with unit circulation, then as $u \rightarrow u_j$, it must be of the form $\phi \propto (u - u_j)$. On the other hand, $\phi(\varphi, z)$ must be a linear combination of the basis functions $\{e^{im\varphi}, m \in \mathbb{Z}\}$, due to the periodicity along φ . This implies that the phase winding of $\phi(\varphi, z)$ is of the form

$$\phi(\varphi, z) \propto W_j^\pm, \quad W_j^\pm = (e^{\pm iu} - e^{\pm iu_j}); \quad u = \varphi + i\frac{2S}{\nu}z. \quad (7)$$

Their corresponding superfluid velocities are

$$\mathbf{v}_s = \nabla\Theta_j^\pm, \quad \Theta_j^\pm = \arg(W_j^\pm). \quad (8)$$

Note that both W_j^+ and W_j^- have the same $+2\pi$ circulation, since both reduce to $u - u_j$ as $u \rightarrow u_j$. Their velocity profiles, however, are very different. The gradients,

$$\partial_\varphi\Theta_j^\pm = \mp \frac{e^{\pm(2S/\nu)(z-z_j)} - \cos(\varphi - \varphi_j)}{2[\cosh\frac{2S}{\nu}(z-z_j) - \cos(\varphi - \varphi_j)]}, \quad (9)$$

$$\partial_z\Theta_j^\pm = \frac{2S}{\nu} \frac{\sin(\varphi - \varphi_j)}{2[\cosh\frac{2S}{\nu}(z-z_j) - \cos(\varphi - \varphi_j)]}, \quad (10)$$

show that $\nabla\Theta_j^+$ and $\nabla\Theta_j^-$ are related by a π rotation about the vortex core. Far from the vortex core, they approach a constant on one side and vanish on the other,

$$\nabla\Theta_j^+ \rightarrow \begin{cases} -1 \cdot \hat{\varphi} & z \gg z_j \\ 0 & z \ll z_j, \end{cases} \quad \nabla\Theta_j^- \rightarrow \begin{cases} 0 & z \gg z_j \\ 1 \cdot \hat{\varphi} & z \ll z_j, \end{cases} \quad (11)$$

as shown in Figs. 2(a) and 2(b). Because of this feature, we refer to Θ_j^+ and Θ_j^- as the *A* and *B* vortex as their velocities are mostly nonvanishing ‘‘above’’ and ‘‘below’’ the vortex core, respectively. It is easy to see that vortices with ℓ

circulation will also come in two different types: $(e^{\pm iu} - e^{\pm iu_j})^\ell$.

The presence of two types of vortices of the same circulation marks a key difference between the cylindrical and the planar BEC. In the latter case, there is one typical vortex with $+2\pi$ circulation, of the form $x + iy$. This difference can be traced back to the conformal map $w = e^{cu}$ that takes a 2D plane (w_x, w_y) into a cylinder (φ, z) , and c is a complex number that describes the change in scale and orientation of the cylindrical strip with respect to the (w_x, w_y) plane. However, since the wave function of the BEC is made up of the basis functions $\{e^{im\varphi}\}$, c can only be $\pm i$ for vortices of unit circulation, reducing the infinite number of mapping down to 2. The periodicity of the basis function, which exists in all Landau levels, reflects the underlying topology of the cylindrical surface.

Vortex array on a cylindrical surface.—The condensate wave function is $\phi = \sqrt{n} \exp(i\Theta)$, where n is the density profile and Θ is its phase function. For a condensate containing vortices, its wave function can be approximated as $\sqrt{n} = \sqrt{n_{\text{TF}}}f$, where n_{TF} is the Thomas-Fermi (TF) density profile in the absence of vortices and f is a function that is 1 everywhere except within a region of the size of the coherence length around the vortex singularity. In our calculations, we shall use the variational form

$$f(u) = \prod_j \tanh\frac{|u - u_j|}{\xi} \quad (12)$$

for a system with vortices located at u_j , where ξ is the core size, also written in units of R . This form has been shown to match well with experiment for rotating gases [24]. For a condensate with *A* vortices at points $(\{u_j, j = 1, \dots, Q\})$ and *B* vortices on another set of points $(\{u_{j'}, j' = 1, \dots, Q'\})$, we take the following variational form of phase function Θ :

$$\exp(i\Theta) = W/|W|, \quad W = \prod_{j=1}^Q W_j^+ \prod_{j'=1}^{Q'} W_{j'}^-. \quad (13)$$

The entire variational wave function is therefore specified by the total number of particles (which fixes the chemical potential and hence n_{TF} [20]), and the location of vortices.

With the variational wave function $\phi = \sqrt{n_{\text{TF}}}f \exp(i\Theta)$, the energy in Eq. (2) becomes a function of the coordinates (φ_j, z_j) of the vortices [20]. We have searched for the minimum of this function numerically by varying the vortex locations. Since the system has reflection symmetry in the z direction, *A* and *B* vortices must appear in pairs at the appropriate location to respect this symmetry. Our results are shown in Fig. 3. We have found that for $S \leq 4$, the gauge field is not strong enough to generate vortices in the ground state. For $S = 5, 6, 7, 8$, there are 4, 6, 8, 10 vortices, respectively, lying on the circle at $z = 0$

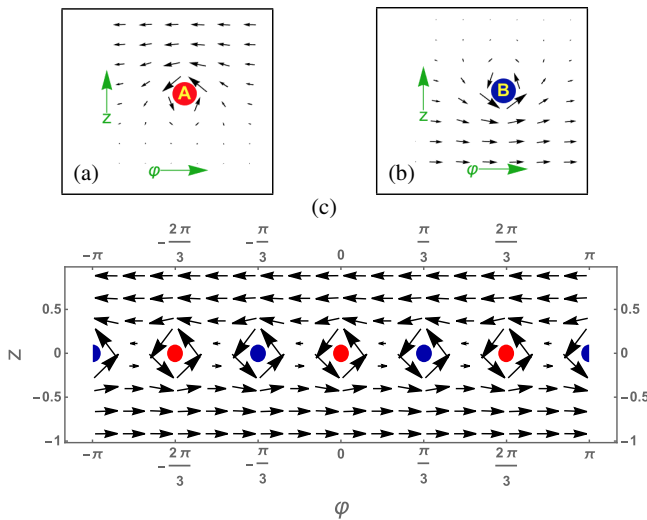


FIG. 2 (color online). (a),(b) Velocity profiles for the *A* and *B* vortex, respectively. The velocity of the *A* (or *B*) vortex reaches a constant above (below) the vortex core and vanishes below (above) it over a distance of R . (c) Velocity profile of a necklace of six alternating *AB* vortices. It is equivalent to the velocity profile of two countercirculating superfluid rings.

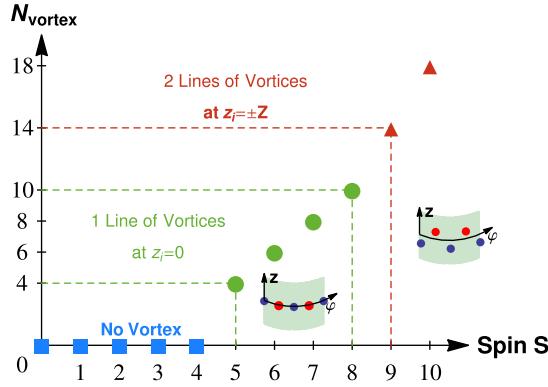


FIG. 3 (color online). For $S \leq 4$, the ground state contains no vortex. Within $S = 5, 6, 7, 8$, the vortices aligned in one row at $z_i = 0$ with the pattern $A-B-A-B$. For $S \geq 9$, the vortices array splits into two rows centering at $z_i = \pm Z$, with all A vortices aligned in one row and all B vortices in another.

(i.e., $z_j = 0$). These “necklaces” of vortices are all in the alternating pattern $A-B-A-B$..., with equal spacing. For $S \geq 9$, the vortices split into two rows, with the A vortices shifted above and the B vortices shifted below $z = 0$ [20].

The reason that the vortex pattern is so different from the planar case is a consequence of the confining geometry (lack of trapping potential along the φ direction). We can see the connection of the necklace pattern to the usual hexagonal pattern in the following hypothetical process. Assuming S can be increased continuously, the vortices will grow in number and will split into more and more necklaces. The hexagonal array is the limit where the number of necklaces approaches the number of vortices within one necklace. The $S = 9$ example in Fig. 3 can be viewed as a tendency towards the hexagonal lattice limit.

To conclude, we examine the phase function and velocity field of the alternating vortex row in greater detail. Let us consider the case of $S = 6$ (corresponding to ^{168}Er), where the ground state has a necklace of 6 equally spaced, alternating A and B vortices at $z = 0$ and $\varphi = n(2\pi/6)$, where $n = 0, 1, \dots, 5$. Defining $w = e^{iu} = e^{i\varphi - (2S/\nu)z}$ and $\alpha = e^{2\pi/6}$, the phase function W in Eq. (13) is

$$W = \prod_{n=0,1,2} [(w - \alpha^{2n})(w^{-1} - \alpha^{-(2n+1)})] = w^3 - w^{-3}. \quad (14)$$

The wave function is then

$$\phi(\varphi, z) \sim \sqrt{1 - z^2} f(\varphi, z) \frac{e^{3i\varphi - 3z(2S/\nu)} - e^{-3i\varphi + 3z(2S/\nu)}}{|e^{3i\varphi - 3z(2S/\nu)} - e^{-3i\varphi + 3z(2S/\nu)}|}. \quad (15)$$

For $z > 0$ ($z < 0$), $\phi(\varphi, z)$ quickly approaches $e^{-3i\varphi}$ ($e^{3i\varphi}$). The system is essentially two countercirculating superflows above and below $z = 0$, as shown in Fig. 2(c).

Signature of the vortex array.—The presence of these alternating vortex array can be detected in time-of-flight experiments. As we have discussed, a necklace of $2n$ vortices will generate two counterphase superflows $e^{-in\varphi}$ and $e^{+in\varphi}$ for $z > 0$ and $z < 0$. The system can be approximated by two rings of condensates with opposite circulation, with one ring sitting above the other along z with a separation of the order of their radius R . In the time-of-flight experiment, these two rings will produce an interference at the $z = 0$ plane of the form $e^{-in\varphi} + e^{+in\varphi}$ and exhibit a density pattern with $2n$ -fold symmetry. This effect is in fact found in an explicit calculation of the ballistic expansion of the vortex row condensate in Eq. (15). The time evolution of the condensate is given by

$$\phi(\mathbf{x}, t) = \int_{-1}^1 dz \int_{-\pi}^{\pi} d\varphi U(\varphi, z, t; \varphi', z') \phi(\varphi', z'), \quad (16)$$

where $U(\varphi, z, t; \varphi', z')$ is the Green function for free-particle propagation at large distance and at long times in cylindrical coordinates, $U(\varphi, z, t; \varphi', z') \approx \exp\{-i[Rr \cos(\varphi - \varphi') + (2S/\nu)^2 z z'] / x_0^2\}$, and $x_0 = \sqrt{\hbar t/m}$. The density pattern at the equatorial plane $z = 0$ at long times is shown in Fig. 4. Experimentally, the density of the expanded cloud in the equatorial plane (at $z = 0$) can be measured by first using a sheet of light to excite the original atoms (denoted as “ a ”) in this plane to a different atomic state (say, “ b ”), and then image the atoms in the b state afterwards.

Concluding remarks.—The emergence of two kinds of vortices with identical vorticity in a cylindrical manifold is a new feature of Bose condensates in a cylinder. It is a consequence of the topological constraint on the single

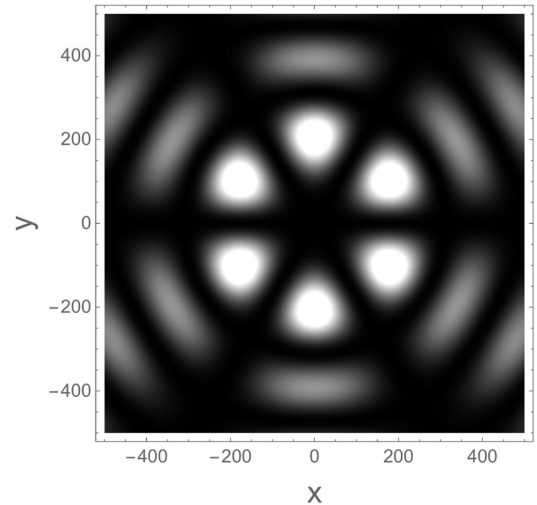


FIG. 4. The time-of-flight image of the vortex row in Fig. 2(c), taken at the time t such that $x_0/R = \sqrt{\hbar t/m}/R = 7$ on the x - y plane at $z = 0$. Length is measured in units of R . The $2n$ -fold symmetry of the image reflects the number of vortices in the vortex row.

valueness of the wave function (i.e., that forces the spatial dependence to be expressed in terms of $e^{i\varphi}$), which will persist even when the manifold is deformed. Although we focus on a particular aspect of the quantum gas in curved surfaces, there are a lot more to explore, especially for systems with greater complexity. Realization of quantum gases in curved surfaces will surely open an exciting direction for cold atom research.

This work is supported by NSF Grant No. DMR-1309615, MURI Grant No. FP054294-D, and NASA Grant No. 1501430.

-
- [1] X. G. Wen and A. Zee, *Phys. Rev. Lett.* **69**, 953 (1992).
 [2] J. E. Avron, R. Seiler, and P. G. Zograf, *Phys. Rev. Lett.* **75**, 697 (1995); N. Read, *Phys. Rev. B* **79**, 045308 (2009); N. Read and E. H. Rezayi, *Phys. Rev. B* **84**, 085316 (2011).
 [3] F. de Juan, A. Cortijo, and M. A. H. Vozmediano, *Phys. Rev. B* **76**, 165409 (2007).
 [4] See N. Cooper, *Adv. Phys.* **57**, 539 (2008); A. L. Fetter, *Rev. Mod. Phys.* **81**, 647 (2009), and the references therein.
 [5] M. R. Matthews, B. P. Anderson, P. C. Haljan, D. S. Hall, M. J. Holland, J. E. Williams, C. E. Wieman, and E. A. Cornell, *Phys. Rev. Lett.* **83**, 3358 (1999).
 [6] K. W. Madison, F. Chevy, W. Wohlleben, and J. Dalibard, *Phys. Rev. Lett.* **84**, 806 (2000).
 [7] J. R. Abo-Shaeer, C. Raman, J. M. Vogels, and W. Ketterle, *Science* **292**, 476 (2001).
 [8] P. Engels, I. Coddington, P. C. Haljan, and E. A. Cornell, *Phys. Rev. Lett.* **89**, 100403 (2002).
 [9] V. Schweikhard, I. Coddington, P. Engels, V. P. Mogendorff, and E. A. Cornell, *Phys. Rev. Lett.* **92**, 040404 (2004).
 [10] M. W. Zwierlein, J. R. Abo-Shaeer, A. Schirotzek, C. H. Schunck, and W. Ketterle, *Nature (London)* **435**, 1047 (2005).
 [11] Y.-J. Lin, R. L. Compton, K. J. Garcia, J. V. Porto, and I. B. Spielman, *Nature (London)* **462**, 628 (2009).
 [12] M. Aidelsburger, M. Atala, M. Lohse, J. T. Barreiro, B. Paredes, and I. Bloch, *Phys. Rev. Lett.* **111**, 185301 (2013).
 [13] C. J. Kennedy, W. C. Burton, W. C. Chung, and W. Ketterle, [arXiv:1503.08243](https://arxiv.org/abs/1503.08243).
 [14] A. Eckardt, C. Weiss, and M. Holthaus, *Phys. Rev. Lett.* **95**, 260404 (2005).
 [15] P. Hauke, O. Tieleman, A. Celi, C. Olschlager, J. Simonet, J. Struck, M. Weinberg, P. Windpassinger, K. Sengstock, M. Lewenstein, and A. Eckardt, *Phys. Rev. Lett.* **109**, 145301 (2012).
 [16] G. Jotzu, M. Messer, R. Desbuquois, M. Lebrat, T. Uehlinger, D. Greif, and T. Esslinger, *Nature (London)* **515**, 237 (2014).
 [17] For recent reviews of synthetic gauge fields, see M. Lewenstein, A. Sanpera, and V. Ahufinger, *Ultracold Atoms in Optical Lattices: Simulating Quantum Many-Body Systems* (Oxford University Press, Oxford, England, 2012); N. Goldman, G. Juzeliunas, P. Ohberg, and I. B. Spielman, *Rep. Prog. Phys.* **77**, 126401 (2014).
 [18] There has been a recent proposal of realizing curved surfaces in the presence of lattice; see O. Boada, A. Celi, J. Rodriguez-Laguna, J. I. Latorre, and M. Lewenstein, *New J. Phys.* **17**, 045007 (2015).
 [19] The cylindrical surface has an extrinsic curvature (radius of the cylinder) but a vanishing intrinsic (or Gaussian curvature). Our results depend on the periodicity of cylinder and the Berry phase of the spins. Since a closed curved surface with genus ≥ 1 must be periodic in some generalized coordinates, it may also have different types of vortices of the same circulation.
 [20] See Supplemental Materials at <http://link.aps.org/supplemental/10.1103/PhysRevLett.115.155304> for more details.
 [21] M. W. Ray, E. Ruokokoski, S. Kandel, M. Mottonen, and D. S. Hall, *Nature (London)* **505**, 657 (2014).
 [22] Near $z = 0$ they have the effect of a harmonic trap: $|\nabla\zeta|^2 + (\zeta^\dagger\nabla\zeta)^2 = (S/2)[(5R^2 + 4z^2)/(R^2 + 4z^2)^2] \approx (S/2R^2)[5 - 32(z/R)^2]$.
 [23] T. L. Ho, *Phys. Rev. Lett.* **87**, 060403 (2001).
 [24] G. Watanabe, S. A. Gifford, G. Baym, and C. J. Pethick, *Phys. Rev. A* **74**, 063621 (2006).